JACS
JOURNAL OF THE AMERICAN CHEMICAL SOCIETY

Article

pubs.acs.org/JACS

Mechanism of Orientation-Dependent Asymmetric Charge Transport in Tunneling Junctions Comprising Photosystem I

Olga E. Castañeda Ocampo,[†,‡,§] Pavlo Gordiichuk,[‡,§] Stefano Catarci,[‡] Daniel A. Gautier,[‡] Andreas Herrmann,*[,‡] and Ryan C. Chiechi*[,†,‡]

[†]Stratingh Institute for Chemistry, University of Groningen, Nijenborgh 4, 9747 AG Groningen, The Netherlands

[‡]Zernike Institute for Advanced Materials, University of Groningen, Nijenborgh 4, 9747 AG Groningen, The Netherlands

Supporting Information

ABSTRACT: Recently, photoactive proteins have gained a lot of attention due to their incorporation into bioinspired (photo)electrochemical and solar cells. This paper describes the measurement of the asymmetry of current transport of self-assembled monolayers (SAMs) of the entire photosystem I (PSI) protein complex (not the isolated reaction center, RCI), on two different "director SAMs" supported by ultraflat Au substrates. The director SAMs induce the preferential orientation of PSI, which manifest as asymmetry in tunneling charge-transport. We measured the oriented SAMs of PSI using eutectic Ga–In (EGaIn), a large-area technique, and conducting probe atomic force microscopy (CP-AFM), a single-complex technique, and determined that the transport properties are comparable. By varying the temperatures at which the measurements were performed, we found that there is no measurable dependence of the current on temperature from ±0.1 to ±1.0 V bias, and thus, we suggest tunneling as the mechanism for transport; there are no thermally activated (e.g., *hopping*) processes. Therefore, it is likely that relaxation in the electron transport chain is not responsible for the asymmetry in the conductance of SAMs of PSI complexes in these junctions, which we ascribe instead to the presence of a large, net dipole moment present in PSI.

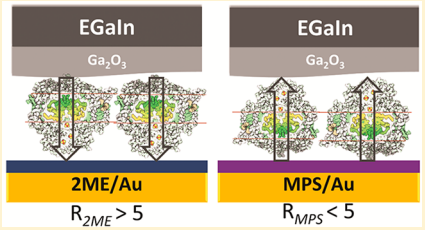

INTRODUCTION

There are two basic strategies for constructing devices in which the flow of electrons is mitigated by single molecules: top-down and bottom-up. Top-down methods rely on nanofabrication or mechanical control to form the nanometer-scale junctions between "top" and "bottom" electrodes necessary to contact molecules end-to-end. Bottom-up methods typically rely on the self-assembly of molecules onto a bottom electrode in which the junction is defined by the molecules themselves when a top electrode (top-contact) is applied; these are devices that, in part, fabricate themselves.[1] Nature provides a plethora of intricate molecular complexes that form by and are prone to self-assembly; however, these complexes are subject to different constraints than their simpler, synthetic counterparts such as the well-studied alkanethiols.[2] Conventional techniques for forming top-contacts for devices or for measuring electrical properties over large areas of self-assembled monolayers (SAMs) of organic molecules have been thus far limited to the direct deposition of metals[3] by electron-beam or thermal evaporation or the addition of an electrically conductive polymer layer between the SAM and a metallic top contact;[4,5] however, in these techniques, the high temperatures, vacuum processing and the need for acidic or organic solvents to spin coat the polymers are not ideal for biomacromolecules. Other, "soft," nondamaging methods for forming top-contacts, such as the use of hanging Hg drops[6] (HMDs), are better suited to this task.[7,8]

Ron et al.[9] used HMDs as a nondamaging method for forming top-contacts to measure the electron transfer (ET) through three protein (complexes) on doped-Si substrates: azurin (Az), bacteriorhodopsin (bR), and bovine serum albumin (BSA), establishing that proteins can function as building blocks for bottom-up tunneling junctions. Although nondamaging, Hg is better suited for Si substrates than metals, with which it tends to form amalgams (Au and Ag are the most common metals used in bottom-up tunneling junctions). These studies on complete proteins were preceded by discussed models of mechanisms of electron transport through peptides and proteins, for example, by Giese et al.[10,11] Waleed Shinawari et al.[12] reviewed biomolecular charge transport, with a particular focus on DNA and protein molecules. A recent progress report by Amdursky et al.[13] compares current densities for different techniques, including CP-AFM and scanning tunneling microscopy (STM) and macroscopic, for junctions comprising proteins and small molecules.

The liquid metal eutectic, Ga–In (which we abbreviate "EGaIn"; 75% Ga, 25% In by weight, mp = 15.5 °C),[14] can function similarly to Hg in the HMD method, but does not form alloys with noble metals.[15] It also exhibits non-Newtonian rheology, driven by a self-limiting oxide,[16] and does not spontaneously reorganize to minimize its surface energy.[15] Thus, it can be formed into stable, nonspherical tips to form ~100 μm^2 contacts and is stable in microfluidic channels, which facilitates variable-temperature measurements.[15,17,18]

Received: February 4, 2015
Published: June 9, 2015

DOI: 10.1021/jacs.5b01241
J. Am. Chem. Soc. 2015, 137, 8419–8427

Photosystem I (PSI) is a complex that houses one of the two reaction centers used in the photosynthetic reactions in cyanobacteria, algae and plants where the conversion of solar energy to electron hole pairs takes place. Isolated PSI complexes from thermophilic unicellular cyanobacterium *Thermosynechococcus elongatus BP-1* have evolutionally formed a trimer structure for improved light absorption efficiency and stability at harsh conditions. The monomer of PSI has a polar stroma and lumen and an apolar backbone. Its size is approximately 13 × 8 × 9 nm and contains 96 light sensitive Chlorophyll *a* (Chl*a*) molecules that are densely packed in the protein scaffold[19] to harvest light. In the complex, harvested photons are converted into excited electrons by chlorophylls at P700 (via a special pair of Chl*a* molecules). This transfer occurs from the primary electron donor complex to the primary electron acceptor A_0 (Chl*a*), to the ferredoxine docking region through the built-in electron transport chain A_1 (phylloquinone), F_X, F_A and F_B (Fe_4S_4 clusters) (Figure 1a). The complex

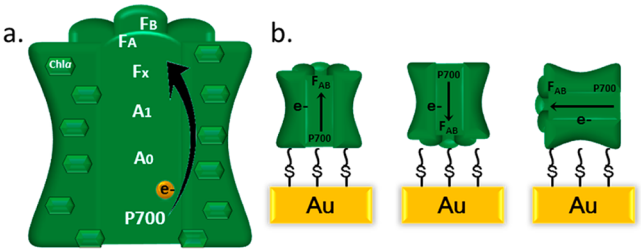

Figure 1. (a) Schematic representation of electron transfer chain in Photosystem I (ET Chain). (b) Possible orientations of PSI on Au surfaced induced by chemical modification. Photosystem I can be anchored in an "up" orientation where the flow is in the opposite direction (P700 adjacent to substrate), a "down" orientation in which the natural direction of the flow of electrons is toward the electrode surface (FB down), or with its electron transport vector parallel to the substrate.

has a photovoltage of 1 V under illumination with an internal quantum efficiency close to unity.[20,21]These features make PSI a unique and interesting protein complex to study. Furthermore, the entire PSI complex, as well as the reaction center (RCI) from plants and cyanobacteria have been extensively characterized and the electrical properties have been observed by a variety of experimental techniques.[19,22−33] We studied the entire PSI complex, not isolated RCI, because it contains the electron transport chain, the light-harvesting array of chlorophylls and the protein scaffold that holds them in place.

We investigated the *J*−*V* characteristics of SAMs of PSI in the dark on template-stripped Au[34] measured by forming top-contacts from tips of EGaIn. EGaIn has been used to measure current density (*J*) versus applied voltage (*V*) through SAMs of a variety of molecules to form rectifiers,[17,35−37] to observe quantum interference effects,[38] to relate dipole moments to vacuum-level shifts,[39] and it is sensitive enough to resolve the odd−even effect in SAMs of alkanethiolates.[40,41] Unlike SAMs of small molecules, however, there are no data from EGaIn tunneling junctions of PSI or any other protein complexes against which to compare. Thus, we characterized SAMs of PSI trimers by interrogating the complexes in the dark, one at a time, by CP-AFM and compared those data to the ensemble averages produced by EGaIn contacts in order to relate our findings to previous studies. We use the asymmetry of the conductance data (i.e., rectification) to elucidate the orientation of PSI because it is self-referencing and, therefore, is less sensitive than the magnitude of *J* to other structural features of the SAM, but very sensitive to the specific geometry of the SAM/EGaIn interface[42] (e.g., orientation). Asymmetry observed in current transport is particularly useful for elucidating the transport properties of protein complexes, which are vastly more complex in structure, size, self-assembly and electrical properties than small molecules, because it eliminates the uncertainty of area calculations that arises from topology, packing density, etc.[36] And while virtually all tunneling junctions with EGaIn top contacts show some asymmetry (because the junction itself is asymmetric), the rectifying behavior of the SAM is readily distinguishable.[43] We are not suggesting that SAMs of PSI make particularly good rectifiers of current—the magnitude of the asymmetry of the current is quite small—only that small changes in asymmetry can provide information about the orientation of PSI complexes.

Photosystem I can be anchored in a "down" orientation in which the natural flow of photogenerated electrons is to the electrode surface (F_B down), an "up" orientation where electrons would flow in the opposite direction (P700 adjacent to substrate), or with its electron transport vector parallel to the substrate (Figure 1b). This level of control over the orientation of the electron transport chain provides an opportunity to determine its role in the tunneling transport through PSI through the self-assembly process rather than by modifying the complexes themselves. Different methods have been used to control the orientation of PSI and RCI on surfaces, ranging from surface modification with different functional groups that interact electrostatically with different parts of the protein complex, to direct covalent attachment via mutation[26] and SAMs with different functional head groups.[28,31] With EGaIn, we can address the monolayers of PSI complexes electrically and from these electrical measurements we can probe the average orientation of the complexes in the monolayer to compare against AFM images and CP-AFM *I*−*V* data.

According to previous reports on single complexes of RCI (i.e., not SAMs or ensembles and not PSI), asymmetric charge transport is completely dependent on the orientation on the surface of the electrode. Greenbaum and co-workers[27,29] were the first to observe this behavior. They platinized one end of the photosynthetic complex and "welded" it to a Au surface using SAMs of small molecules as "director" monolayers.[28] They used scanning tunneling spectroscopy (STS) to examine the electronic properties of each RCI, which elicited orientation-dependent asymmetry. Others subsequently observed this behavior in RCI as single complexes[30] and in SAMs.[31] This phenomenon is easily conflated with light-driven processes,[25] which involves hopping transport (to move through the transport chain as the electron changes in energy) and therefore should not play a role in tunneling measurements. Yet, the absolute orientation of RCI and, by extension, PSI is assigned from STS data based on the assumption that the direction of asymmetry (rectification) follows the electron transport chain.[27,29] By measuring tunneling junctions comprising PSI in the dark, we found that this assignment of the orientation does not, in fact, map onto PSI—it is backward—and that tunneling transport, therefore, likely dominates any hopping contribution from the electron transport chain.

DOI: 10.1021/jacs.5b01241
J. Am. Chem. Soc. 2015, 137, 8419−8427

RESULTS AND DISCUSSION

General Results. We exposed ultraflat template stripped Au (Au^{TS}) substrates to a solution of 1 mM 2-mercaptoethanol (2ME) or sodium 3-mercapto-1-propanesulfonate (MPS) to form "director SAMs" to bias the orientation of PSI trimers that self-assemble on top of these SAMs.[28,31,44] These director SAMs differ in length by 1.7 Å, which may affect the magnitude of the tunneling current, but we do not rely on this magnitude as a measure in this work and small changes in the thickness of the director SAM are unlikely to influence asymmetry. The PSI in cyanobacteria has an asymmetric distribution of surface charges in the stroma and lumen (see Supporting Information for details). Two thirds of all the charged surface residues are concentrated at the "top" of the complex; the stromal, F_{AB} electron acceptor side (Figure 1a). This difference is likely what determines the preferred orientation during self-assembly on modified surfaces. We immobilized PSI on the substrates by drop casting from aqueous buffer and incubating them (i.e., leaving them in contact) for 2 h. We investigated each SAM topographically by AFM and electrically using CP-AFM and EGaIn. The CP-AFM data are averages of $I-V$ curves from 100 complexes for each director SAM. Thus, they sample the distribution of orientations similarly to the large-area EGaIn measurements and can be compared directly. We define the asymmetry of current transport (rectification ratio), R, as the ratio of J or I at positive to negative bias; $R = |J(-)/J(+)|$ for EGaIn and $R = |I(-)/I(+)|$ for CP-AFM, both with respect to the wiring convention for CP-AFM (see Supporting Information).

Measured AFM height profile images show better PSI coverage for 2ME than for MPS, with protein heights close to 6 nm on Au^{TS}. This value is less than the 9 nm thickness derived from the crystal structure data because these SAMs are measured under ambient, anhydrous conditions and contact with the AFM tip can compress them somewhat (for more details see Supporting Information). We imaged individual PSI trimers within SAMs of PSI formed on both directing SAMs by AFM to determine the density (per μm^2) and measured their electrical properties by CP-AFM to determine the orientation of the complexes, assigning low values of R to PSI that is oriented up and high values to down. Values of unity were assigned to PSI that is oriented parallel to the substrate (sideways). The results are summarized in Table 1. (The average values of R for EGaIn and CP-AFM are given in Table 2.) Individual $I-V$ traces were averaged over 100 PSI complexes at different locations within the SAMs.

For EGaIn measurements, the SAMs of PSI on both director SAMs were contacted by lowering a syringe (connected to an electrometer) supporting a tip of EGaIn. Recent reports on EGaIn junctions comprising alkanethiolates employ a slightly different method in which the tips are first flattened against a Si wafer and then pressed into the SAM;[45] however, light contact with as-prepared tips yielded stable and reproducible results on SAMs of PSI. We observed four different behaviors: (i) shorts, characterized by linear $J-V$ curves with currents in the μA regime; (ii) no-contact, characterized by noisy currents in the pA regime; (iii) poor-contact, which begins with no-contact $J-V$ curves, but is followed by shorts after further lowering of the EGaIn tip; and (iv) good contact, characterized by S-shaped $J-V$ curves of reproducible, low-noise currents. The yield of working devices (good contacts) was higher than 70%. These data are summarized in Table 3 and show higher rectification ratio when 2ME is used as opposed to MPS, which we ascribe to the different distributions of orientations of PSI induced by the director SAMs. We analyzed the data identically to the CP-AFM data by averaging log J. See the Supporting Information for a detailed discussion of the data analysis.

Table 1. Percentage of Average Orientation of PSI Depending on the Different Directing SAMs[a]

directing SAM	up (%)	down (%)	sideways (%)	coverage (PSI trimer/μm^2)
MPS	57	18	25	723
2ME	11	69	20	853

[a]The results were obtained by measuring the asymmetry of the $I-V$ curves by CP-AFM. The average coverage on an area of 1 μm^2 was calculated from AFM height images. The table summarizes the statistical distributions of the $I-V$ curves of over 100 points for both director SAMs.

Table 2. Asymmetry (R) of Nonshorting Junctions[a]

method	R MPS (1 V)	R 2ME (1 V)
EGaIn PSI	2.0	5.0
CP-AFM PSI	0.8	1.8
EGaIn deactivated PSI	0.9	1.0

[a]These values were calculated from evaluating $J-V$ curves at ±1 V. $R = |J(-)/J(+)|$ for EGaIn and $R = |I(-)/I(+)|$ for CP-AFM, both with respect to the wiring convention for CP-AFM (see Supporting Information). Values refer to the calculated geometric mean from curves at ±1 V.

Table 3. Characterization of Junctions by Director SAM, Current Density (J), and Percentage of Yield of Nonshorting Junctions[a]

			yield (%)		
method	directing SAM	J (1 V) A/cm^2	good contact	shorts/no contact	poor contact
EGaIn PSI	2ME	1.69×10^{-04}	74	9	17
EGaIn PSI	MPS	1.48×10^{-03}	72	14	14
deactivated PSI	2ME	1.87×10^{-04}	100	0	0
deactivated PSI	MPS	1.57×10^{-04}	100	0	0
no PSI	2ME	2.04	–	–	–
no PSI	MPS	0.020	–	–	–

[a]The values of J are the geometrical averages from measurements with EGaIn tips. The yield of working devices is based on devices with EGaIn as top electrode.

Charge-Transport Occurs through Intact PSI Complexes. As control experiments, we measured the electrical properties of denatured PSI (which are shown in the Supporting Information). We boiled PSI for 20 min at 99 °C, which is sufficient to denature it completely and then prepared SAMs of deactivated PSI by following the same procedures used to prepare SAMs of active PSI. We observed no rectifying behavior in EGaIn junctions comprising boiled PSI, nor did we observe shorts (Table 3). The lack of shorts implies that denatured PSI still covers the substrate, as SAMs of 2ME and MPS are fragile and give mostly shorts. Thus, the origin of the asymmetry is dependent on the presence of intact PSI structures (i.e., the overall asymmetry of the junction depends on the presence of intact complexes of PSI).

DOI: 10.1021/jacs.5b01241
J. Am. Chem. Soc. 2015, 137, 8419−8427

We varied the density (surface coverage) of the SAMs of PSI by preparing PSI trimer solutions of different concentrations (dilutions from 1:1 to 1:130, ratio of concentration of 1 μm PSI to buffer) while keeping the incubation time fixed. From AFM images, we determined the surface coverage by comparing the PSI-covered surface to the total surface area; $\chi_{PSI} = [N \cdot A_{PSI}/A_{total}] \cdot 100\%$ where N is the number density of PSI, A_{PSI} is the area occupied by PSI complexes (25 nm, determined from TEM), A_{total} is the total area investigated. Figure 2 shows the

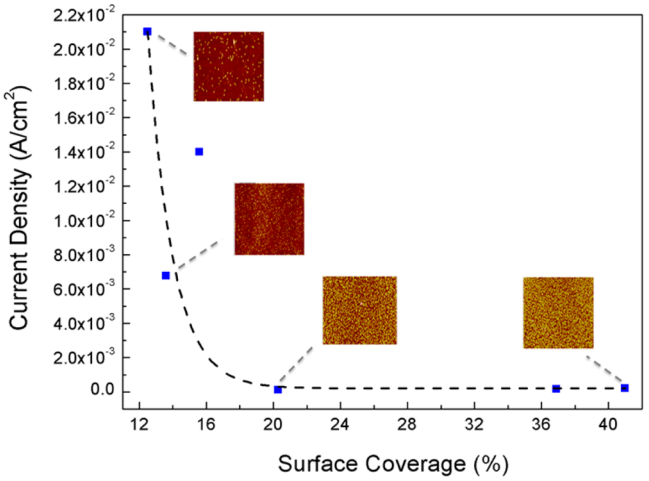

Figure 2. Asymptotic fit of J at 1 V vs percentage of surface coverage for PSI on 2ME as directing SAM. The blue squares are the experimental points. The threshold limit of coverage is 23% as determined by imaging surfaces at different PSI:buffer concentrations and characterizing their behavior with an EGaIn tips. Inset images show PSI complexes on Au^{TS} at different concentrations which correspond to the percent coverages shown. The devices were imaged on an AFM at 2.5 μm.

correlation between χ_{PSI} and the magnitude of J in EGaIn junctions. The exponential relationship between J and surface coverage is further evidence that the charges are flowing through the PSI complexes. Below 23% coverage the junctions become unstable, irreproducible, and yield mostly shorts (as do bare director SAMs). Presumably this percentage is the cutoff value below which EGaIn is able to penetrate between the PSI complexes and contact the director SAM. This behavior is not unlike defect-mediated transport in which the electrical properties of highly conductive defects (space between PSI complexes) become dominant at a critical density.[46] The saturation of J at 23% implies that transport occurs exclusively through PSI and that there is no (or constant) leakage current, which allows the direct comparison of the data from EGaIn and CP-AFM junctions.

To evaluate the influence of contact with tips of EGaIn, we marked areas of the SAMs of PSI and imaged them by AFM before and after forming EGaIn junctions and acquiring J–V data (see Supporting Information). We observed no qualitative damage to the monolayers and, by counting the number of complexes in each junction before and after forming EGaIn junctions, determined that no complexes were extricated from the monolayer. From these experiments we conclude that the SAMs of PSI are not damaged and that the individual complexes do not move and are not removed during measurement. Thus, EGaIn is a demonstrably nondamaging method for investigating charge-transport through SAMs of PSI and is capable of forming reversible junctions, which may be useful for characterizing SAMs of PSI (or other protein complexes) as an intermediate step in the fabrication of devices to, for example, verify the orientation of the complexes.

PSI Rectifies Current. The rectifying behavior of RCI (not PSI) was previously observed by STS[28] and CP-AFM[31] on individual protein complexes. In our studies with EGaIn, PSI assembled on director SAMs exhibited an asymmetric conductance between bias voltages with R = 5.0 with 2ME and 2.0 with MPS (Table 2). The direction of rectification does not invert when the orientation of the complexes is reversed because there is some built-in asymmetry in these junctions; the bottom electrode supports a covalently bound director SAM that supports the PSI complexes, while the top-contact is physisorbed either via contact with an AFM tip or by supporting an EGaIn electrode. Thus, one orientation works with the built-in asymmetry and the other against it, but not sufficiently to overcome it completely.

We ascribe the asymmetry in both cases to the ratio of the orientation of the complexes (Table 1). An important distinction between single-complex studies (e.g., CP-AFM and STS) and large-area studies (e.g., EGaIn and HMD) is that the latter sample the average orientation. Coupled with the ability to measure many locations across many different substrates, large-area measurements are useful for characterizing the self-assembly of PSI (or any protein with direction-dependent rectification). Additionally, the nondamaging nature of EGaIn makes it a useful tool for investigating SAMs of PSI during the fabrication of a thin-film device, for example, a photovoltaic device, the properties of which are dominated by the average orientation of PSI.[47−49] Single-complex measurements provide details that are difficult or impossible to extract from large-area measurements, thus the combination of the two gives a complete picture, capturing the details of transport through individual complexes and the supramolecular structure of the SAM.

Although it is clear that the relative orientation of RCI and PSI is influenced by the chemistry at the surface of the bottom electrode (Au^{TS} in our case), the absolute orientation of either has not been determined unambiguously. It was observed that RCI preferentially platinizes at one side, which was assumed to occur at the more polar (electron accepting) side of the complex.[27] Despite the lack of direct evidence, this one study has become the reference point for the absolute orientation of RCI and, by extension, PSI. Our data were acquired on SAMs of PSI, which has a different electrostatic profile than RCI and therefore does not necessarily orient identically to RCI.

We propose two possible mechanisms for rectification. The first is that charges (electrons or holes) take advantage of the electron transport chain or directly traverse it; both mechanisms involve thermally activated hopping processes. These mechanisms (it is not clear specifically which) are used to infer the absolute orientation of RCI and predict higher values of R when PSI is oriented up. The second mechanism assumes that tunneling charges do not hop through electron transport pathway and the rectification is instead driven by the large dipole moment of the whole PSI structure between the luminal and the stromal surface (i.e., perpendicular to the substrate when PSI is in the up or down orientation). Van Haeringen et al. used linear dichroism to elucidate the dipole moment within the structure of trimeric PSI.[50] The direction of the dipole is parallel to the C3-symmetry axis of the protein trimer complex, with positive side of the dipole moment on the

DOI: 10.1021/jacs.5b01241
J. Am. Chem. Soc. 2015, 137, 8419−8427

luminal side and negative on the stromal side. The dipole effect within PSI trimers was also observed on solid-state bulk heterojunction (BHJ) solar cells with a work function shift.[47] (There, a monolayer of PSI trimers was self-assembled at a metal-oxide electrode rather than Au.) The electric field of this dipole moment can either enhance or oppose the total field created by biasing the electrodes as is shown in Figure 3. This

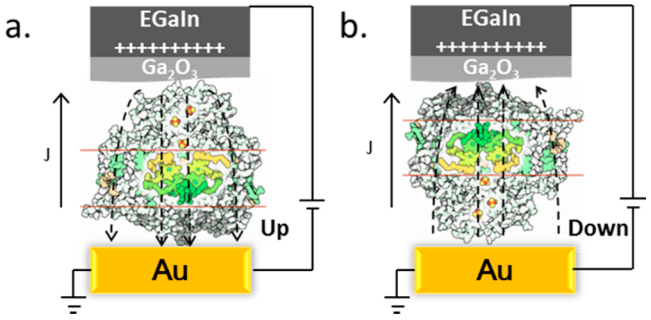

Figure 3. Direction of the electrical field (dashed lines) that arises from the PSI dipole moment within PSI-EGaIn devices, which are shown with EGaIn biased positively (with respect to the normal wiring of EGaIn). The direction of this field goes from negative to positive in the complex. (a) When PSI is oriented "up", the electric field from the applied bias opposes the internal electric field of the PSI complexes. (b) When PSI is oriented "down," the direction of the internal electric field is the same as the applied bias. Thus, this mechanism predicts that PSI in the down orientation will give higher values of *R*.

mechanism would show higher values of *R* when PSI is oriented down. Although we have no way to observe the absolute up/down orientations of PSI directly, we can assign the absolute orientation by determining which mechanism (the electron transport chain or the internal electric field) is more likely. First, however, we must establish that CP-AFM and EGaIn are in agreement in order to relate our observations to previous reports (which exist for CP-AFM, but not for EGaIn).

EGaIn and CP-AFM Data Are Directly Comparable. Although the influence of the native oxide layer on EGaIn has been thoroughly studied on aliphatic SAMs and has been shown to have a negligible influence on transport properties,[16] it is necessary to confirm that the same holds true for protein complexes. Due to the size of complexes of PSI, we are able to isolate individual complexes for CP-AFM measurements, meaning that the calculation of per-complex resistivity is unambiguous. For EGaIn junctions, we know the density of PSI complexes and the measured contact area, A_{geo}, but not the actual contact area, A_{eff}, which is considerably smaller due to the topology of the EGaIn tip.[45] Thus, we can calculate the number of complexes in A_{geo}, compute the resistance and determine the correction factor to relate A_{geo} and A_{eff}. If the oxide is benign in this study, this correction should be comparable to the values reported for aliphatic SAMs.

For a given EGaIn junction, we considered every oriented PSI complex as a resistor in parallel. We calculated the resistance of individual complexes (R_i) from average values of *I* from CP-AFM measurements at 1 V (range of ~10^9 to 10^{10} Ohms depending on the orientation). The resistance, R_{obs}, is the total resistance of the circuit and, at $V = 1$ V, is the reciprocal of the current calculated for an area with *n* number of complexes, allowing the calculation of *n* from eq 1 where I_{EGaIn} is the measured current of an EGaIn/Ga_2O_3//PSI junction.

$$\frac{V}{R_{obs}} = I_{EGaIn} = \sum_{1}^{n} \frac{1}{R_i} \quad (1)$$

The values of *n* given by eq 1 are 4.5 and 2.2×10^2 for 2ME and MPS, respectively. Using these values of *n*, we calculated A_{eff} from the densities of PSI complexes shown in Table 1. From the measured value of A_{geo}, eq 2 gives the overestimation of the area, α.

$$\frac{A_{geo}}{A_{eff}} = \alpha \quad (2)$$

From this calculation we find $\alpha \sim 10^3$, which is consistent with the values of ~10^4 that have been observed for aliphatic SAMs.[45,51] Thus, using the per-complex conductivity determined by CP-AFM and the magnitude of the current obtained from large-area measurements with EGaIn, we arrive at a value of α that is within a factor of 10 of previously reported values. This result shows that the contact resistance associated with the physisorbed electrode-PSI interface is comparable for EGaIn/Ga_2O_3 and a Pt/Ir CP-AFM tip and, therefore, that the influence of the oxide layer on charge-transport is negligible (i.e., it does not contribute to R_{obs} more than a CP-AFM tip); CP-AFM and EGaIn data are comparable. This results is unsurprising in the context of existing studies on SAMs of alkanethiolates,[43] but it is necessary to establish the benign nature of the oxide specifically in junctions incorporating proteins.

Using our computed value of α, we plotted the per-complex current-densities from CP-AFM and EGaIn (Figure 4c,d). The values of *R* from EGaIn are in agreement with the values of *R* from CP-AFM data, but Figure 4c,d also shows a qualitative agreement between the line shapes. For comparison reasons we added the averaged *I*−*V*, *J*−*V* curves with respect to the original wiring for CP-AFM and EGaIn, respectively (Figure 4a,d).

While EGaIn junctions cannot be scanned past ±1 V without precipitating shorts (from electrostatic pressure), CP-AFM junctions can be scanned further because the height of the tip is fixed by the instrument rather than the SAM of PSI. Thus, while the CP-AFM and EGaIn data are in remarkably close agreement at ±1 V, we cannot know for certain that they would not diverge at higher potentials.

The Mechanism of Charge-Transport Is Tunneling. Cahen and co-workers have shown, using HMDs, that the electrical properties of junctions comprising metalloproteins are affected by the removal of the metal centers.[9] These studies show that tunneling electrons can take advantage of the accessible states of the metal centers. In studies of RCI (not PSI) where rectification is observed, the mechanism is almost always ascribed to the electron transport chain;[27−31] however, no evidence is offered to support or refute that hypothesis. Previous studies have shown that, when the electron transport chain is deliberately engaged, the rate of electron transfer in RCI is higher from P700 to F_{AB} (forward) than in the reverse direction,[23,52] which could explain the diode-like behavior seen in the *J*−*V* curves.[29] The two most straightforward experiments for establishing the mechanism are removing the electron transport chain and variable-temperature studies. The former is not possible without substantially influencing the structure of RCI/PSI, and the latter is not possible with the techniques that have been used to study RCI thus far. Fortunately, the (remarkable) robustness of SAMs of PSI in vacuo[47] extends to sufficiently low temperatures to enable variable-temperature

DOI: 10.1021/jacs.5b01241
J. Am. Chem. Soc. 2015, 137, 8419−8427

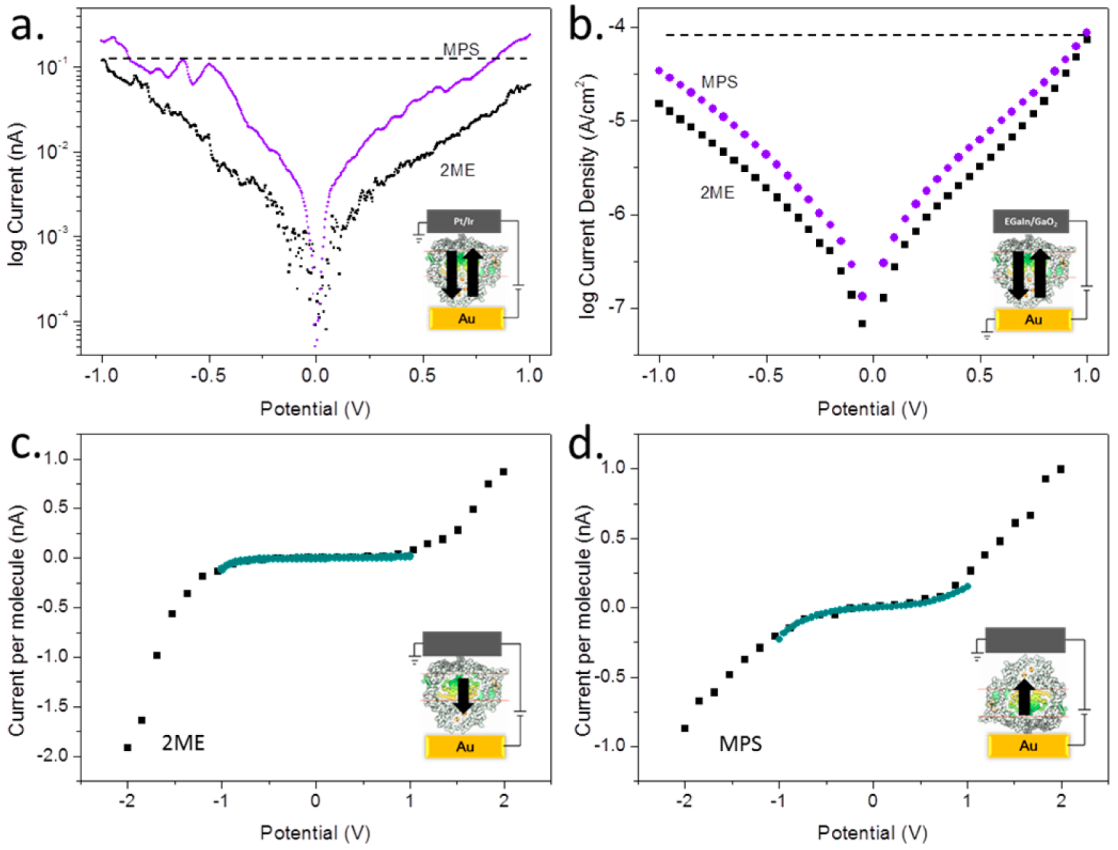

Figure 4. Top: Semilog plots of current and current density versus voltage for junctions measured using CP-AFM (a) and EGaIn (b) for SAMs of PSI on MPS (purple) and 2ME (black) The black arrows indicate the orientation of the PSI complexes on the surface. These data are plotted according to the normal wiring of each technique (see the Supporting Information for details). The horizontal, dashed lines are to guide the eye. Bottom: Per-complex $J-V$ curves for SAMs of PSI on 2ME (c) and MPS (d) measured by CP-AFM (black squares) and EGaIn (green circles) plotted with respect to the standard wiring of CP-AFM (shown in the insets). Per-complex values of J for EGaIn were calculated using number densities of PSI measured by AFM and a correction factor for the difference between the measured and effective area of the EGaIn junctions.

studies using microfluidic channels filled with EGaIn in a crossbar configuration.[15]

One of the most robust rectifying tunneling junctions comprises ferrocene-terminated SAMs on Ag with EGaIn top-contacts.[17,35−37] The mechanism of rectification in these SAMs is the (partial) pinning of the HOMO of the ferrocene to EGaIn, which pushes it either into or out of resonance with a Ag^{TS} electrode depending on the sign of the applied potential on EGaIn; when it moves into resonance (negative potential), charges tunneling onto the HOMO and then hops onto the EGaIn, shortening the effective tunneling distance. This mechanism was proven by Arrhenius plots (ln $|J|$ vs $1/T$), which clearly show the "freezing out" of the hopping component, leading to the loss of rectification at temperatures below the activation energy of the hopping process.[17] If the mechanism of rectification in PSI involves thermally activated hopping processes in the electron transport chain, it should freeze out as well. Thermally activated transport processes have also been observed in CP-AFM studies of long conjugated molecules[53,54] and proteins such as azurin,[55,56] ferritin,[57] and cytochrome[58] at elevated temperatures. We did not collect transport data above room temperature, but at low temperature we observed comparable results. Thus, there may be temperature-dependent transport pathways at elevated temperatures, but they do not contribute to the asymmetric transport at room temperature.

If the mechanism of rectification in our PSI junctions involves the electron transport pathway then it must also involve a hopping process, as the electrons change energy inside the complexes; moving with the electron transport chain (downhill) then leads to higher values of J than against it (uphill) at a particular value of $|V|$. If, however, the mechanism of rectification is the interaction of the applied field with the built-in field of the collective dipole moments of the PSI complexes, the process is entirely *tunneling*; the rectification arises from the different probabilities of tunneling from left to right and right to left. The former mechanism, therefore, will show a loss of rectification at low temperatures as the hopping processes are frozen out, while the latter will be completely independent of temperature.

We fabricated microfluidic devices following literature procedures and acquired $J-V$ traces at different temperatures. An Arrhenius plot of ln $|J|$ at ± 0.50 V for PSI on both directing SAMs is shown in Figure 5 (the raw data are shown in the Supporting Information). The magnitude of R, shown by the difference in the magnitude of J at positive and negative bias, is invariant with temperature. The values of ln $|J|$ are also nearly invariant, showing only a slight perturbation only near room temperature. These data are unambiguous evidence that the mechanism of charge transport through SAMs of PSI on MPS and 2ME is independent of temperature and, therefore, that the mechanism of rectification does not involve *hopping* and/or the electron transport chain. From this conclusion, we can ascribe

DOI: 10.1021/jacs.5b01241
J. Am. Chem. Soc. 2015, 137, 8419−8427

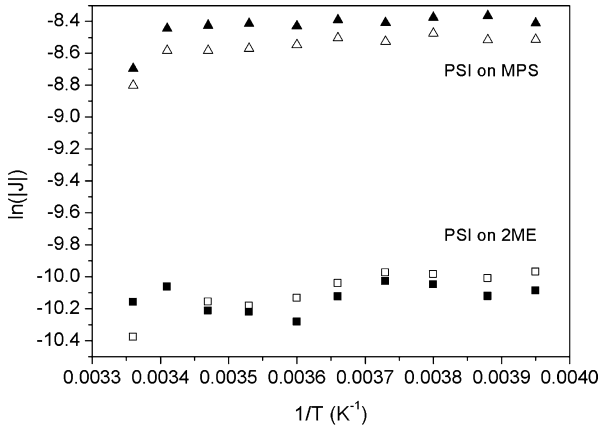

Figure 5. ln |*J*| at ±0.50 V as a function of inverse temperature for PSI on directing SAMs of MPS (triangles) and 2ME (squares). The solid symbols (▲, ■) represent the positive bias (+0.50 V) and hollow (□, Δ) represent the negative bias (−0.50 V). The linearity indicates that the mechanism of charge transport is dominated by *tunneling* as no temperature dependence was measured. The entirety of the curves for biases from −1 to 1 V can be found on the Supporting Information.

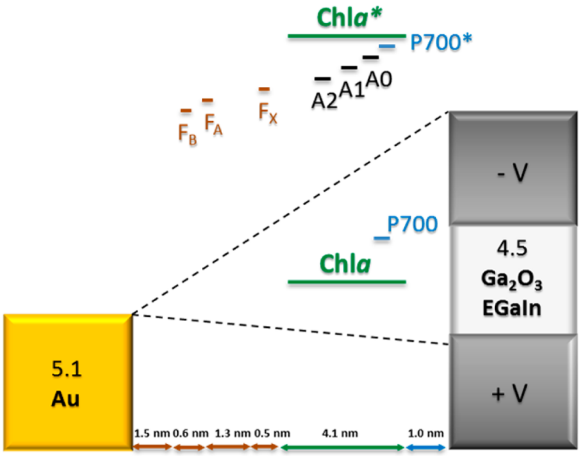

Figure 6. Energy level diagram across Au^{TS}-PSI(P700/F_B)//Ga_2O_3/EGaIn junctions. The barrier width is defined by the thickness of one oriented PSI complex, which is depicted in the "down" orientation with respect to the natural direction of electron flow. The green lines are the frontier orbital energies of the chlorophyll molecules, which are distributed evenly through the thickness of the PSI complex. The black lines represent the energies of the electron transport chain and their relative spatial positions. On the basis of the orientation of the electron transport chain, more current should flow when the EGaIn electrode is biased negatively than at the equivalent positive bias. That mechanism would translate into higher values of *R* when the complexes are oriented "up" (because this figure is drawn with respect to the wiring of EGaIn junctions; Figure 4 shows the data with respect to the wiring diagram of CP-AFM). However, in our experiments we observe more current at the positive bias, which supports our dipole moment hypothesis. The distances between cofactors were estimated with the software PyMOL from a crystal structure of PSI taken from the Protein Data Bank (1JB0).

an absolute orientation of PSI; it is oriented "down" (P700 adjacent to the EGaIn substrate) on 2ME and "up" on MPS. Thus, the direction of rectification is exactly opposite to the natural flow of electrons through the electron transport chain, which predicts higher currents at positive bias (with respect to EGaIn) when P700 is adjacent to the EGaIn electrode. An energy level diagram based on Nakamura's et al. observation[21] is shown in Figure 6. It not only predicts that asymmetry will be more pronounced in the up orientation, but that $R < 1$. Note that this diagram is drawn with respect to the normal wiring of EGaIn and is, therefore, backward from the wiring convention of CP-AFM.

A common test for tunneling transport is to compare the decay coefficient, β, against literature values. This value is obtained from Simmons' approximation, $J = J_0 e^{-\beta d}$, where d is distance between the electrodes and β is obtained by varying d. This study is not possible with PSI because d is fixed by the complex at 6 nm. Ron et al. estimated β by comparing I in the presence and absence of a protein, arriving at values of 0.18, 0.12, and 0.27 $Å^{-1}$ for three different proteins on Si surfaces modified with octadecyltrimethoxysilane.[9] Using the same analysis, we arrive at a value of 0.16 for PSI on 2ME and 0.08 $Å^{-1}$ for PSI on MPS with $\Delta d = 60$ Å and values of J taken from Table 3.

To gain more experimental insight into the mechanism of rectification, we measured the transport properties of bovine and human serum albumin (BSA and HSA), which have been studied extensively.[13,55,59−61] We observed $R \sim 5.5$ and 3.0 on 2ME and MPS, respectively (see Supporting Information). This observation can only be reconciled using the mechanism of rectification proposed in this paper, given that SAMs of BSA and HSA show preferential ordering[62] and that they contain only alpha helices, which contribute to a collective dipole moment. It also explains the observation by Ron et al. that BSA rectifies on Br-terminated Si surfaces using HMD electrodes.[9]

■ CONCLUSIONS

We have established a clear relationship between the average orientation of PSI (not RCI) in SAMs and the asymmetry (rectification) of current in metal/protein/metal junctions on template-stripped Au surfaces modified with directing SAM. Asymmetry is a useful observable for capturing the complexities of assemblies of large, biological molecules, particularly in combination with single-complex measurements, which are insensitive to collective properties, but which provide details that are missed by large-area methods. The average orientation is affected by the identity of the directing SAM used to control the surface chemistry of the substrate.

Through variable-temperature measurements we have established that the dominant mechanism of charge-transport through SAMs of PSI on Au is likely *tunneling* and that, at the very least, it does not involve thermally activated transport. This observation refutes the hypothesis that rectification is due to the natural direction of the flow of electrons through the transport chain, which involve thermally activated processes, and instead is likely the result of the internal electric field that arises from the collective action of dipoles (and multipoles) in the peptide backbone. It opposes the natural direction of electron flow through the electron transport pathway and therefore predicts that 2ME preferentially orients PSI "down" and MPS "up" with respect to the direction of the flow of electrons through the transport chain in vivo; i.e., with P700 adjacent to the EGaIn substrate. This assignment of the orientations of PSI is in agreement with solid-state, thin-film devices comprising PSI (not RCI) that is oriented by modifying the surface of the bottom electrode.[47,49]

DOI: 10.1021/jacs.5b01241
J. Am. Chem. Soc. 2015, 137, 8419−8427

EXPERIMENTAL SECTION

Fabrication of Solid-State Devices. We thermally deposited a 120 nm-thick layer of gold (Au 111) onto a technical-grade 3′′ silicon wafer supporting a native oxide layer (Si/SiO_2). We fabricated the substrates by template stripping (TS),[34] where a drop of ultraviolet (UV)-curable optical adhesive (OA) was used to adhere a 1 × 1 cm piece of glass to a preprepared gold coated wafer. The glass was then mechanically cleaved exposing an ultraflat Au surface with a root-mean-squared roughness of 0.3 nm (as measured using tapping-mode AFM).

Next, we immersed the substrates in a solution of 1 mM 2-mercaptoethanol (2ME) or sodium 3-mercapto-1-propanesulfonate (MPS) to direct the PSI complexes to adopt a down or up orientation (F_B iron−sulfur cluster adjacent or away from substrate). The time of immersion was limited to 2 h to avoid the formation of multilayers or aggregates. After this step, were rinsed the substrates with MQ water (MPS) or ethanol (2ME), dried them with nitrogen and incubated them in a previously prepared PSI solution.[47] The PSI solution consisted of 1:1 in buffer A (20 mM HEPES (pH 7.5); 10 mM $MgCl_2$; 10 mM $CaCl_2$; 500 mM Mannitol with 0.05% DDM (*n*-Dodecyl-*β*-D-maltoside)) for 2 h. They were then rinsed with MQ water and dried with nitrogen.

Monolayer Surface Characterization. We analyzed each substrate by AFM after each fabrication step: on the template-stripped substrate after cleavage, after surface modification, and after incubation in a solution of PSI.

We used the resulting images to measure the surface coverage of PSI. This analysis revealed a true surface coverage of up to 50%. This was calculated by knowing the diameter of the PSI trimer from TEM images and the coverage density (calculated manually) for specific areas. We obtained the AFM images with MultiMode 8 with ScanAsyst Microscope in tapping mode with TESP probes (Bruker) with spring constant k = 42 N·m^{-1}, resonance frequency f = 320−410 kHz and tip radius of less than 10 nm. The scan rate and resolution were 1 Hz and 640 lines/sample, respectively. We analyzed the AFM images with the software NanoScopeAnalysis 1.2 from Bruker.

We studied the conductivity of the immobilized PSI on the two orienting monolayers with AFM Tunneling Atomic Force Microscopy (TUNA) contact mode with a conducting probe. This mode was applied for electrical characterization of single (trimer) PSI complex with Pt/Ir coated Si n-type probe (APPNano), spring constant k = 0.02−0.8 N·m^{-1}, resonance frequency f = 5−25 kHz and tip radius less than 30 nm with contact resistance of 0.01−0.025 ohm/cm. Statistic data was performed over 100 independent measured points for each orienting SAM. The applied force to CP-AFM conducting probe on top of PSI was started from low and step-by-step increased to reach contacting for I−V recording. This approach was used for each measurement point with forces of less than 10 nN.

Electrical Measurements. We formed the EGaIn electrodes by suspending a drop of EGaIn from a 10 mL syringe on an adjustable stage. Using a piezo stepper (open-loop, ∼5 nm resolution) we brought the drop into contact with the SAM of PSI. The EGaIn adhered to both the needle and the Au and by retracting the needle slowly (ca. 50 μms^{-1}, we produced conical tips of EGaIn with diameters of ∼25 μm in diameter.[14,38]

We performed the electrical measurements in a custom-built Faraday cage using a Keithley 6430 Sub-Femtoamp Remote SourceMeter SMU Instrument. The device was held in place with a spring-loaded gold tip that was isolated from ground. Bias was applied to a syringe filled with EGaIn. Data were obtained from an average of points by sweeping the potential from −1.0 to 1.0 V at a rate of 0.2 V/s.

Fabrication of Soft Devices for Variable-Temperature Measurements. To elucidate the transport mechanism of bacterial PSI-based devices, we measured the dependence of the electric behavior on temperature. In order to do this, we fabricated encapsulated and addressable devices able to operate in a pressure and temperature controlled setup[17] (see Supporting Information).

ASSOCIATED CONTENT

Supporting Information

Details on the acquisition and processing of data, control experiments, monolayer formation, device fabrication, variable temperature measurements, electrical wiring and activity measurements of PSI. The Supporting Information is available free of charge on the ACS Publications website at DOI: 10.1021/jacs.5b01241.

AUTHOR INFORMATION

Corresponding Authors

*a.herrmann@rug.nl

*r.c.chiechi@rug.nl

Author Contributions

§O.E.C.O. and P.G. contributed equally to the research.

Notes

The authors declare no competing financial interest.

ACKNOWLEDGMENTS

This work was supported by the Zernike Institute for Advanced Materials "Dieptestrategie". RCC also acknowledges the European Research Council for ERC Starting Grant 335473 (MOLECSYNCON).

REFERENCES

(1) Zhang, Y.; Zhao, Z.; Fracasso, D.; Chiechi, R. C. *Isr. J. Chem.* **2014**, *54* (5−6), 513−533.

(2) Love, J. C.; Estroff, L. A.; Kriebel, J. K.; Nuzzo, R. G.; Whitesides, G. M. *Chem. Rev.* **2005**, *105* (4), 1103−1169.

(3) Haick, H.; Ghabboun, J.; Cahen, D. *Appl. Phys. Lett.* **2005**, *86* (4), 042113.

(4) Milani, F.; Grave, C.; Ferri, V.; Samorì, P.; Rampi, M. A. *ChemPhysChem* **2007**, *8* (4), 515−518.

(5) Akkerman, H. B.; Blom, P. W. M.; de Leeuw, D. M.; de Boer, B. *Nature* **2006**, *441* (7089), 69−72.

(6) Ellis, W. D. *J. Chem. Educ.* **1973**, *50* (3), A131.

(7) Rampi, M. A.; Whitesides, G. M. *Chem. Phys.* **2002**, *281* (2−3), 373−391.

(8) Simeone, F. C.; Rampi, M. A. *Chimia* **2010**, *64* (6), 362−369.

(9) Ron, I.; Sepunaru, L.; Itzhakov, S.; Belenkova, T.; Friedman, N.; Pecht, I.; Sheves, M.; Cahen, D. *J. Am. Chem. Soc.* **2010**, *132* (12), 4131−4140.

(10) Giese, B.; Eckhardt, S.; Lauz, M. In *Encyclopedia of Radicals in Chemistry, Biology and Materials*; Chatgilialoglu, C., Studer, A., Eds.; John Wiley & Sons, Ltd.: Chichester, U.K., 2012.

(11) Giese, B.; Graber, M.; Cordes, M. *Curr. Opin. Chem. Biol.* **2008**, *12* (6), 755−759.

(12) Waleed Shinwari, M.; Jamal Deen, M.; Starikov, E. B.; Cuniberti, G. *Adv. Funct. Mater.* **2010**, *20* (12), 1865−1883.

(13) Amdursky, N.; Marchak, D.; Sepunaru, L.; Pecht, I.; Sheves, M.; Cahen, D. *Adv. Mater.* **2014**, *26* (42), 7142−7161.

(14) Chiechi, R. C.; Weiss, E. A.; Dickey, M. D.; Whitesides, G. M. *Angew. Chem., Int. Ed.* **2008**, *47* (1), 142−144.

(15) Dickey, M. D.; Chiechi, R. C.; Larsen, R. J.; Weiss, E. A.; Weitz, D. A.; Whitesides, G. M. *Adv. Funct. Mater.* **2008**, *18* (7), 1097−1104.

(16) Cademartiri, L.; Thuo, M. M.; Nijhuis, C. A.; Reus, W. F.; Tricard, S.; Barber, J. R.; Sodhi, R. N. S.; Brodersen, P.; Kim, C.; Chiechi, R. C.; Whitesides, G. M. *J. Phys. Chem. C* **2012**, *116* (20), 10848−10860.

(17) Nijhuis, C. A.; Reus, W. F.; Barber, J. R.; Dickey, M. D.; Whitesides, G. M. *Nano Lett.* **2010**, *10* (9), 3611−3619.

(18) So, J.-H.; Dickey, M. D. *Lab. Chip* **2011**, *11* (5), 905.

(19) Jordan, P.; Fromme, P.; Witt, H. T.; Klukas, O.; Saenger, W.; Krauß, N. *Nature* **2001**, *411* (6840), 909−917.

(20) Croce, R.; van Amerongen, H. *Photosynth. Res.* **2013**, *116* (2−3), 153−166.

DOI: 10.1021/jacs.5b01241
J. Am. Chem. Soc. 2015, 137, 8419−8427

(21) Nakamura, A.; Suzawa, T.; Kato, Y.; Watanabe, T. *Plant Cell Physiol.* **2011**, *52* (5), 815−823.
(22) Brettel, K.; Leibl, W. *Biochim. Biophys. Acta* **2001**, *1507* (1−3), 100−114.
(23) Golbeck, J. H. *Annu. Rev. Plant Physiol. Plant Mol. Biol.* **1992**, *43* (1), 293−324.
(24) Das, R.; Kiley, P. J.; Segal, M.; Norville, J.; Yu, A. A.; Wang, L.; Trammell, S. A.; Reddick, L. E.; Kumar, R.; Stellacci, F.; Lebedev, N.; Schnur, J.; Bruce, B. D.; Zhang, S.; Baldo, M. *Nano Lett.* **2004**, *4* (6), 1079−1083.
(25) Gerster, D.; Reichert, J.; Bi, H.; Barth, J. V.; Kaniber, S. M.; Holleitner, A. W.; Visoly-Fisher, I.; Sergani, S.; Carmeli, I. *Nat. Nanotechnol.* **2012**, *7* (10), 673−676.
(26) Carmeli, I.; Frolov, L.; Carmeli, C.; Richter, S. *J. Am. Chem. Soc.* **2007**, *129* (41), 12352−12353.
(27) Lee, I.; Lee, J. W.; Warmack, R. J.; Allison, D. P.; Greenbaum, E. *Proc. Natl. Acad. Sci. U. S. A.* **1995**, *92* (6), 1965−1969.
(28) Lee, I.; Lee, J.; Greenbaum, E. *Phys. Rev. Lett.* **1997**, *79* (17), 3294−3297.
(29) Lee, J. W.; Lee, I.; Greenbaum, E. *Biosens. Bioelectron.* **1996**, *11* (4), 375−387.
(30) Stamouli, A.; Frenken, J. W. M.; Oosterkamp, T. H.; Cogdell, R. J.; Aartsma, T. J. *FEBS Lett.* **2004**, *560* (1), 109−114.
(31) Takeshi Mikayama, K. I. *J. Nanosci. Nanotechnol.* **2009**, *9* (1), 97−107.
(32) Frolov, L.; Rosenwaks, Y.; Carmeli, C.; Carmeli, I. *Adv. Mater.* **2005**, *17* (20), 2434−2437.
(33) Reiss, B. D.; Hanson, D. K.; Firestone, M. A. *Biotechnol. Prog.* **2007**, *23* (4), 985−989.
(34) Hegner, M.; Wagner, P.; Semenza, G. *Surf. Sci.* **1993**, *291* (1−2), 39−46.
(35) Nijhuis, C. A.; Reus, W. F.; Whitesides, G. M. *J. Am. Chem. Soc.* **2010**, *132* (51), 18386−18401.
(36) Nijhuis, C. A.; Reus, W. F.; Whitesides, G. M. *J. Am. Chem. Soc.* **2009**, *131* (49), 17814−17827.
(37) Nijhuis, C. A.; Reus, W. F.; Siegel, A. C.; Whitesides, G. M. *J. Am. Chem. Soc.* **2011**, *133* (39), 15397−15411.
(38) Fracasso, D.; Valkenier, H.; Hummelen, J. C.; Solomon, G. C.; Chiechi, R. C. *J. Am. Chem. Soc.* **2011**, *133* (24), 9556−9563.
(39) Fracasso, D.; Muglali, M. I.; Rohwerder, M.; Terfort, A.; Chiechi, R. C. *J. Phys. Chem. C* **2013**, *117* (21), 11367−11376.
(40) Thuo, M. M.; Reus, W. F.; Nijhuis, C. A.; Barber, J. R.; Kim, C.; Schulz, M. D.; Whitesides, G. M. *J. Am. Chem. Soc.* **2011**, *133* (9), 2962−2975.
(41) Yoon, H. J.; Bowers, C. M.; Baghbanzadeh, M.; Whitesides, G. M. *J. Am. Chem. Soc.* **2014**, *136* (1), 16−19.
(42) Jiang, L.; Yuan, L.; Cao, L.; Nijhuis, C. A. *J. Am. Chem. Soc.* **2014**, *136* (5), 1982−1991.
(43) Reus, W. F.; Thuo, M. M.; Shapiro, N. D.; Nijhuis, C. A.; Whitesides, G. M. *ACS Nano* **2012**, *6* (6), 4806−4822.
(44) Yamanoi, Y.; Terasaki, N.; Miyachi, M.; Inoue, Y.; Nishihara, H. *Thin Solid Films* **2012**, *520* (16), 5123−5127.
(45) Simeone, F. C.; Yoon, H. J.; Thuo, M. M.; Barber, J. R.; Smith, B.; Whitesides, G. M. *J. Am. Chem. Soc.* **2013**, *135* (48), 18131−18144.
(46) Weiss, E. A.; Chiechi, R. C.; Kaufman, G. K.; Kriebel, J. K.; Li, Z.; Duati, M.; Rampi, M. A.; Whitesides, G. M. *J. Am. Chem. Soc.* **2007**, *129* (14), 4336−4349.
(47) Gordiichuk, P. I.; Wetzelaer, G.-J. A. H.; Rimmerman, D.; Gruszka, A.; de Vries, J. W.; Saller, M.; Gautier, D. A.; Catarci, S.; Pesce, D.; Richter, S.; Blom, P. W. M.; Herrmann, A. *Adv. Mater.* **2014**, *26* (28), 4863−4869.
(48) Darby, E.; LeBlanc, G.; Gizzie, E. A.; Winter, K. M.; Jennings, G. K.; Cliffel, D. E. *Langmuir* **2014**, *30* (29), 8990−8994.
(49) Yu, D.; Wang, M.; Zhu, G.; Ge, B.; Liu, S.; Huang, F. *Sci. Rep.* **2015**, *5*, 9375.
(50) Van Haeringen, B.; Dekker, J. P.; Bloemendal, M.; Rögner, M.; van Grondelle, R.; van Amerongen, H. *Biophys. J.* **1994**, *67* (1), 411−417.
(51) Sangeeth, C. S. S.; Wan, A.; Nijhuis, C. A. *J. Am. Chem. Soc.* **2014**, *136* (31), 11134−11144.
(52) Lee, J. W.; Lee, I.; Laible, P. D.; Owens, T. G.; Greenbaum, E. *Biophys. J.* **1995**, *69* (2), 652−659.
(53) Luo, L.; Choi, S. H.; Frisbie, C. D. *Chem. Mater.* **2011**, *23* (3), 631−645.
(54) Choi, S. H.; Frisbie, C. D. *J. Am. Chem. Soc.* **2010**, *132* (45), 16191−16201.
(55) Li, W.; Sepunaru, L.; Amdursky, N.; Cohen, S. R.; Pecht, I.; Sheves, M.; Cahen, D. *ACS Nano* **2012**, 121114092743005.
(56) Sepunaru, L.; Friedman, N.; Pecht, I.; Sheves, M.; Cahen, D. *J. Am. Chem. Soc.* **2012**, *134* (9), 4169−4176.
(57) Rakshit, T.; Banerjee, S.; Mukhopadhyay, R. *Langmuir* **2010**, *26* (20), 16005−16012.
(58) Amdursky, N.; Ferber, D.; Bortolotti, C. A.; Dolgikh, D. A.; Chertkova, R. V.; Pecht, I.; Sheves, M.; Cahen, D. *Proc. Natl. Acad. Sci. U. S. A.* **2014**, *111* (15), 5556−5561.
(59) Amdursky, N.; Pecht, I.; Sheves, M.; Cahen, D. *J. Am. Chem. Soc.* **2012**, *134* (44), 18221−18224.
(60) Amdursky, N.; Ferber, D.; Pecht, I.; Sheves, M.; Cahen, D. *Phys. Chem. Chem. Phys.* **2013**, *15* (40), 17142.
(61) Amdursky, N.; Pecht, I.; Sheves, M.; Cahen, D. *Proc. Natl. Acad. Sci. U. S. A.* **2013**, *110* (2), 507−512.
(62) Mentovich, E. D.; Belgorodsky, B.; Kalifa, I.; Cohen, H.; Richter, S. *Nano Lett.* **2009**, *9* (4), 1296−1300.

DOI: 10.1021/jacs.5b01241
J. Am. Chem. Soc. 2015, 137, 8419−8427